ASIA-PACIFIC JOURNAL OF CHEMICAL ENGINEERING
Asia-Pac. J. Chem. Eng. 2010; **5**: 35–47
Published online 2 September 2009 in Wiley InterScience
(www.interscience.wiley.com) DOI:10.1002/apj.380

Curtin University of Technology

Special Theme Review

Production of ultrapure hydrogen in a Pd–Ag membrane reactor using noble metal supported on La-based oxides. Modeling for the dry reforming of methane reaction

*J. F. Múnera, L. Coronel, B. Faroldi, C. Carrara, E. A. Lombardo and L. M. Cornaglia**

Instituto de Investigaciones en Catálisis y Petroquímica (FIQ, UNL-CONICET), Santiago del Estero 2829, 3000 Santa Fe, Argentina

Received 1 September 2008; Revised 9 November 2008; Accepted 13 November 2008

ABSTRACT: A review is presented here of our previous contributions concerning the production of ultrapure hydrogen through the dry reforming of methane conducted in a membrane reactor. The reaction equilibration ratio is the criterion to compare the catalytic performance of the La-based catalysts used in these studies. The solids were characterized by Laser Raman, X- ray photoelectron spectroscopy, X-ray diffraction and temperature-programmed reduction. The different behaviors are discussed taking into account the characterization results. To predict the influence of key process variables on conversion and product composition, a mathematical model is proposed to simulate the membrane reactor built around a palladium–silver membrane with 100% hydrogen selectivity. This study uses the kinetic equations developed for the dry reforming reaction on a Rh/La_2O_3 catalyst. © 2009 Curtin University of Technology and John Wiley & Sons, Ltd.

KEYWORDS: membrane reactor; methane; Rh; Ru

INTRODUCTION

Catalytic dry reforming is the reaction of carbon dioxide with methane to produce syngas. If the main goal is to produce H_2, this reaction can be carried out in a membrane reactor (MR) combining the reaction and the purification in a single vessel. This system offers the possibility of overcoming the thermodynamic limitations of this endothermic reaction, allowing the attainment of higher methane conversions at lower temperatures.

Several articles have lately appeared on MRs for the methane dry reforming reaction employing different types of membranes and catalysts, such as Pd-ceramic composite membrane and Pt, Ru, Pd, Rh, Ir/Al_2O_3 catalysts[1]; silica/mullite membrane (3 Al_2O_3-2 SiO_2) and Pt/Al_2O_3 catalyst[2]; Pd film supported on porous stainless steel and Ni catalysts[3]; alumina membrane with Ru deposition as catalyst[4]; SiO_2/alumina membrane and Rh/Al_2O_3 catalyst.[5] All of them report an increase in the methane conversion when extracting H_2 from the reaction medium, but only Lee *et al*.[5] and Ferreira-Aparicio *et al*.[3] employed highly selective membranes. Their results depended on the conditions under which the reactions were carried out such as Catalyst Weight/reactant Feed (W/F), dilution of the $CO_2 + CH_4$ mixture, membrane selectivity and its permeation capacity, carbon deposition of the catalyst that would contribute to its deactivation and membrane deterioration.

In our group, we have employed a dense Pd/Ag membrane with 100% selectivity toward hydrogen to produce ultrapure hydrogen. To optimize the MR operation, a balance between the hydrogen produced and the hydrogen removed is a necessary condition.[6] Dalmon *et al*.[7] sustained that the choice of the catalysts may be non-trivial for dehydrogenation reactions carried out in MRs. However, this topic has been underestimated in the last few years. In most cases, a suitable catalyst has to be designed, with long-term stability and no carbon deposition.

Previous studies in fixed-bed reactors (FBR)[8,9] have shown that noble metals like platinum, rhodium and ruthenium are more active than Ni for the methane reforming reactions. Furthermore, when the appropriate supports are used, these formulations are catalytically stable and do not produce a significant amount of carbonaceous residues.

In La-containing noble metal catalysts, we reported[10–13] a high stability attributed to the metal–support interaction. For Ru and Rh/La_2O_3 solids, this

**Correspondence to*: L. M. Cornaglia, Instituto de Investigaciones en Catálisis y Petroquímica (FIQ, UNL-CONICET), Santiago del Estero 2829, 3000Santa Fe, Argentina.
E-mail: lmcornag@fiq.unl.edu.ar

© 2009 Curtin University of Technology and John Wiley & Sons, Ltd.

interaction was very strong. However, when a composite $La_2O_3-SiO_2$ material was used as support, a weaker interaction was observed.[13]

The effect of lanthanum on the activity of metal supported catalysts was recently reported.[14,15] The addition of La_2O_3 on the Al_2O_3 supported Pd catalyst resulted in an increase of the turnover rate for the steam reforming of methane assigned to changes in the Pd structure with blockage of Pd sites.[14] In the case of Ni catalysts, the La_2O_3 content tuned the Ni particle sizes and Ni–H species amounts on the catalysts that led to a higher reforming activity.[15]

The lanthanum Ni-based perovskites are characterized by significant resistance to coking.[16,17] When subjected to reduction processes, perovskite-type oxides produce very small metal particles, in the order of nanometers, with high metallic dispersion.[16] In addition, the partial substitution of Ni by a second metal may inhibit coke formation. For example, the presence of Rh improved catalytic performance by enhancing nickel reduction and dispersion. The catalyst stability was attributed to the formation of a $La_2O_2CO_3$ phase which enhances the removal of carbonaceous deposits, and to the presence of filamentous carbon which does not directly deactivate the catalyst.[17]

Partially substituted perovskites $La_{(1-x)}Ce_xNiO_3$ have been investigated for this reaction.[18] The increase in catalytic activity and inhibition of carbon formation were explained in terms of the Reverse Water Gas Shift (RWGS) reaction which is favored on a Ce-enriched surface found in the perovskite oxide and also by the concerted action of the perovskite structure, providing well-dispersed Ni metal.

We have previously used the following reaction equilibration ratio

$$\eta = \frac{p_{CO}^2 \cdot p_{H_2}^2}{p_{CH_4} \cdot p_{CO_2}} \cdot \frac{1}{K_{eq}}$$

to compare the behavior of different La-based Rh catalysts in a MR. This ratio was defined for the carbon dioxide reforming reaction ($CH_4 + CO_2 \leftrightarrow 2CO + 2H_2$). The best performing formulation was obtained using the composite $La_2O_3-SiO_2$ support. For this catalyst, the reaction equilibration ratio remained constant and close to 1 with the increase of the sweep gas (SG) flow rate when appropriate W/F was applied, indicating that the $Rh/La_2O_3-SiO_2$ catalyst was able to restore the equilibrium even at high SG flow rates.

A good reactor model is required to predict the influence of key process variables on conversion and product composition for a given hydrogen selective membrane. Many researchers have implemented mathematical models to simulate the behavior of MRs.[19,20] However, only Prabhu *et al*.[21] developed a model for the dry reforming reaction using MRs. They incorporated a nonselective porous glass and a highly selective silica modified membrane. Their model showed good agreement with the experimental results.

In what follows, our previous research related to hydrogen production in MRs is revisited. The reaction equilibration ratio is used to evaluate the catalytic behavior of the La-based catalysts. The solids are characterized by laser Raman spectroscopy (LRS), X-ray photoelectron spectroscopy (XPS), X-ray diffraction (XRD), Fourier transform infrared spectroscopy (FTIR) and temperature-programmed reduction (TPR). The different behaviors are discussed taking into account the characterization results. Furthermore, a mathematical model is proposed to simulate the MR built around a palladium–silver membrane with 100% hydrogen selectivity. This study uses the kinetic equations obtained by Múnera *et al*.[22] for the dry reforming on a Rh/La_2O_3 catalyst.

EXPERIMENTAL

Catalyst preparation

The La_2O_3-based catalysts were prepared by the conventional wet impregnation of La_2O_3 (Anedra 99.99%) using either $RuCl_3 \cdot 3H_2O$ (Alfa 99.9%), $H_2(PtCl_6) \cdot 6H_2O$ (99.9%) or $RhCl_3 \cdot 3H_2O$ (Alfa 99.9%). The resulting suspension was then heated at 353 K to evaporate the water, and the solid material was dried in an oven at 383 K overnight.

The $La_2O_3-SiO_2$ support was prepared by incipient wetness impregnation of SiO_2 with lanthanum nitrate (Anedra). The SiO_2 (Aerosil 300) employed in the solid preparation was previously calcined at 1173 K. The La loading was 27.0 wt% of La_2O_3. The solids were calcined at 873 K. The $Rh/La_2O_3-SiO_2$ catalysts were prepared by incipient wetness impregnation using $RhCl_3 \cdot 3H_2O$. The samples were kept at room temperature for 4 h and then dried at 343 K overnight.

All catalysts, independently of the preparation method or the used support, were calcined for 6 h at 823 K in flowing air. Prior to the reaction, they were heated in Ar flow to 823 K and then reduced at the same temperature in H_2 flow for 2 h.

Stability tests

The catalyst (50 mg) was loaded into a tubular quartz reactor (inner diameter, 5 mm) which was placed in an electric oven. A thermocouple in a quartz sleeve was placed on top of the catalyst bed. After reduction, the temperature was adjusted in flowing Ar to the reaction temperature, and the reactant gas mixture (P_{CO_2}: P_{CH_4}: $P_{Ar} = 1:1:1.1$, $P = 1$ atm, W/F $= 4.5 \times 10^{-6}$ g h ml^{-1}) was fed to the reactor. The reaction products

© 2009 Curtin University of Technology and John Wiley & Sons, Ltd.

DOI: 10.1002/apj

were analyzed in a thermal conductivity detector (TCD) gas chromatograph (Shimadzu GC-8A) equipped with a Porapak column, and a molecular sieve column.

Kinetic measurements

Kinetic studies under differential conditions were conducted in the same conventional flow system. The mass of catalyst used was 20–50 mg. This was diluted with 50 mg of inert powder quartz to avoid temperature gradients. Conversions were usually controlled to be significantly lower ($\leq$6%) than those defined by thermodynamic equilibrium by adjusting the total flow rate (187 ml/min) and varying the partial pressures of CH_4 (P_{CH_4}) and CO_2 (P_{CO_2}). Rate limitation by external and/or internal mass transfer under differential conditions proved to be negligible by applying suitable experimental criteria.

Membrane reactor

The double tubular MR was built using a commercial dense Pd–Ag alloy (inner tube, thickness = 50 μm), provided by REB Research and Consulting, with one end closed and an inner tube to allow Ar SG flow rate. The outer tube was made of commercial nonporous quartz (i.d. 9 mm). The catalyst (1 g), diluted with quartz chips (2 g), was packed in the outer annular region (shell side). The inner side of the membrane in all runs was kept at atmospheric pressure. More details have been previously reported.[11] To measure the equilibrium conversions, the MR was operated with neither SG nor pressure difference between the tube and the shell sides. The conversions were measured after a 12-h stabilization period. The reaction products and the permeated mixture were analyzed with a TCD gas chromatograph equipped with a Porapak and a molecular sieve column and with an on-line Balzers Quadstar TU 422 quadrupole mass spectrometer previously calibrated for each gas. The carbon balance was close to one in all cases.

Catalyst characterization

Metal dispersion

The metal dispersion of the fresh catalyst, following the hydrogen reduction at 823 K for 2 h, was determined by static equilibrium adsorption of either H_2 or CO at 373 K in a conventional vacuum system. The CO uptakes were calculated taking into account the three CO adsorption states (linear, bridge and gem) construction. The contribution of each one was evaluated by a fit of the CO adsorption FTIR bands using Lorentzian functions. More details are given elsewhere.[13]

XRD

The XRD patterns of the calcined and used solids were obtained with an XD-D1 Shimadzu instrument, using Cu Kα radiation at 30 kV and 40 mA. The scanning rate was 1.0°/min for values between $2\theta = 10°$ and 70°.

TPR

An Ohkura TP-20022S instrument equipped with a TCD was used for the TPR experiments. To eliminate the carbonates present in the samples, the following pretreatment was used: the samples were heated up to 823 K in oxygen flow, kept constant for one hour and then cooled down in Ar flow. Afterwards, they were reduced in a 5%H_2–Ar stream, with a heating rate of 10 K/min up to the maximum treatment temperature.

Thermogravimetric analysis (TGA)

The absence of carbon on the used catalysts was determined by oxidizing the carbon in a Mettler Toledo TGA/Simultaneous Differential Thermal Analysis (SDTA) (Model 851) system. The used catalysts (usually 10 mg) were heated at 10 K min^{-1} to 1173 K in a flow of 90 ml min^{-1} air. The carbon detection limit was 0.06 μg/mg of catalyst.

XPS

The Rh solid XPS measurements were carried out using a PHI model 1257 electron spectrometer. Non-monochromatic Al Kα X-ray radiation was used. The photoelectron kinetic energy was measured with a hemispheric analyzer in 46.95 eV/step pass energy. In the case of the Ru catalyst, the XPS measurements were performed using an Axis Ultra Kratos electron spectrometer with a non-monochromatic Mg Kα X-ray source (10 kV, 15 mA). All the XPS analyses were performed on the calcined solid and on the used catalyst exposed to air. The pressure in the analysis chamber was about 1×10^{-7} Pa during spectra collection. The spectral regions corresponding to La 3d, Si 2p, O 1s, C 1s, Ru 3d or Rh 3d core levels were recorded for each sample. The peak areas were determined by integration employing a Shirley-type background. Peaks were considered to be a mixture of Gaussian and Lorentzian functions in a 70/30 ratio. For the quantification of the elements, sensitivity factors provided by the manufacturers were used.

LRS

The Raman spectra were recorded with a TRS-600-SZ-P Jasco Laser Raman instrument, equipped with a charge coupled device with the detector cooled to about 153 K using liquid N_2. The excitation source was the 514.5 nm line of a Spectra 9000 Photometrics Ar ion laser. The laser power was set at 30 mW.

© 2009 Curtin University of Technology and John Wiley & Sons, Ltd.

DOI: 10.1002/apj

Table 1. Catalytic performance of Rh, Ru and Pt solids in a fixed-bed reactor.

Catalysts[a]	TOF_{CH_4}[b] (s^{-1})	r_{CH_4}[b]	r_{CO_2}[b]	r_{CH_4}[c]	r_{CO_2}[c]	Dispersion
$Pt(0.93)/La_2O_3$	4.1	0.12	0.27	0.09	0.19	0.17[d]
$Rh(0.2)/La_2O_3$	3.6	0.16	0.33	0.16	0.32	0.64[d]
$Rh(0.6)/La_2O_3$	6.1	0.18	0.45	0.18	0.44	0.14[d]
$Rh(0.6)/La_2O_3-SiO_2$	1.8	0.30	0.61	0.33	0.64	0.79[e]
$Ru(0.6)/La_2O_3$	–	0.21	0.40	0.21	0.44	0.05[d,e]
$Ru(1.2)/La_2O_3$	–	0.25	0.48	0.24	0.50	–

[a] Solids were reduced *in situ* at 823 K before reaction. Wt% of metal and La_2O_3 are given between parentheses. The $La_2O_3-SiO_2$ support was calcined at 873 K.
[b] Reaction rates measured at 823 K after 1 h on stream (mol h^{-1} g^{-1}).
[c] Reaction rates measured at 823 K, W/F = 1.05×10^{-5} g h ml^{-1}, after 100 h on stream.
[d] Obtained by H_2 chemisorption.
[e] Obtained by CO chemisorption.

REVIEW OF OUR FINDINGS

Catalyst stability

Table 1 presents CH_4 and CO_2 reaction rates after 1 h and 100 h on stream for our La-based catalysts. The catalyst stability experiments were performed at 823 K in a FBR. The CO_2 reaction rate was higher than the CH_4 reaction rate due to the occurrence of the RWGS reaction in which CO_2 reacted with the H_2 produced in the reforming reaction; this is consistent with H_2/CO ratios lower than unity (not shown). The stoichiometry of these reactions demands that $H_2/CO = (3 - r_{CO_2}/r_{CH_4})/(1 + r_{CO_2}/r_{CH_4})$ where r_{CH_4} and r_{CO_2} are the experimental CH_4 and CO_2 reaction rates, respectively.[23] This ratio was satisfied for all the measured points.

The $Rh(0.6)/La_2O_3-SiO_2$ solid showed reaction rates higher than those supported on lanthanum oxide. The metal dispersion is a critical parameter in catalytic behavior. The incorporation of the promoter (La_2O_3) to the silica support induced a parallel increase in the metal dispersion that would be responsible for the high reaction rates. However, the Turn Over Frequency (TOF) values decreased with the increasing dispersion of rhodium. The low-TOF values suggest that the activity of the rhodium sites is lower than in the case of the Rh/La_2O_3 solids. Yokota *et al*.[24] correlated the different TOFs with the stabilized species of Rh atom using X-ray Absorption Fine Structure (XAFS) measurement. They concluded that the supports influenced the electronic state of Rh atoms, and that the Rh metal catalyzed the dry reforming reaction as a prominent active species. Appropriate techniques such as XPS will allow to discuss the differences between the Rh active sites on lanthanum-based catalysts.

The Rh and Ru solids remained stable for more than 100 h at $P_{CO_2}/P_{CH_4} = 1$. However, the Pt catalyst exhibited a significant loss of activity after 24 h on stream. To identify the causes of the high stability of the Rh and Ru La-based solids, several characterization techniques were applied. The main results obtained are shown in the following sections.

Metal and lanthanum species in calcined and used catalysts

In La-based systems, several chemical species can be present such us La_2O_3, $La(OH)_3$, $La_2(CO_3)_3$ and $La_2O_2CO_3$.[25] Lanthanum oxycarbonates exist in three crystalline modifications (**I, Ia** and **II**); the three polymorphs hold in an arrangement of ($La_2O_2^{2+}$) layers separated by CO_3^{2-} ions. Type **I** has square layers and is tetragonal, while type **Ia** is described as a monoclinic distortion of form **I**.[26] **II**-$La_2O_2CO_3$ is completely indexed in the hexagonal unit cell.

The characterization of crystalline phases on the lanthanum support and the Ru, Rh and Pt catalysts was performed by XRD, LRS and FTIR. TPD and TGA also contributed to a better understanding of these solids. In this review, the most significant results are presented to sustain our main conclusions. Table 2 summarizes the lanthanum phases detected in the studied solids. The XRD patterns for the calcined catalysts supported on La_2O_3 showed the presence of **II**-$La_2O_2CO_3$ and $La(OH)_3$ phases. La_2O_3 signals were also detected on the Pt(0.93) solid. No XRD reflections associated with noble metal compounds were detected in any case.[27,28]

No Raman data have been found in the literature for $La_2O_2CO_3$ previous to our work. The oxycarbonate Raman spectra show bands in the 250–450 cm^{-1} region.[28] These bands have been assigned to the La–O fundamental modes. Beside, the signals in the 700–1500 cm^{-1} region correspond to the vibration of $CO_3^{=}$ groups.

The Laser Raman spectra of Rh and Ru catalysts exhibit peaks at 358, 384, 747 and 1086 cm^{-1} assigned to type **II** oxycarbonate. In the case of the Pt catalyst, the spectrum also shows weak bands associated with type **Ia** oxycarbonate. When we employed LRS to characterize the Ru–lanthanum system, a broad Raman

© 2009 Curtin University of Technology and John Wiley & Sons, Ltd.

DOI: 10.1002/apj

Table 2. Physicochemical characterization of the catalysts.

Catalysts	Temperature-programmed reduction		X-ray diffraction[b]	Laser Raman spectroscopy
	T[a]	H_2/Metal		
Pt(0.93)/La_2O_3	410(sh) 528 618	2.17	**II**-$La_2O_2CO_3$, La_2O_3, $La(OH)_3$	**II**-$La_2O_2CO_3$ **Ia**-$La_2O_2CO_3$
Rh(0.2)/La_2O_3	433 490	0.82	**II**-$La_2O_2CO_3$, $La(OH)_3$	**II**-$La_2O_2CO_3$
Rh(0.6)/La_2O_3	420 458	1.40	**II**-$La_2O_2CO_3$, $La(OH)_3$	**II**-$La_2O_2CO_3$
Rh(0.6)/La_2O_3–SiO_2	420	1.47	$La_2Si_2O_7$	–
Ru(0.6)/La_2O_3	413(sh) 533 648	1.5	**II**-$La_2O_2CO_3$, $La(OH)_3$	**II**-$La_2O_2CO_3$ Ru(III)species
Ru(1.2)/La_2O_3	413 481 533 (sh)	1.5	**II**-$La_2O_2CO_3$, $La(OH)_3$	Ru(III) species

[a] Maximum temperature (K) of the H_2 consumption peak.
[b] Joint committee on powder diffraction standards (JCPDS): **II**-$La_2O_2CO_3$ (37–804), $La(OH)_3$ (36–1481 and 6–0585), La_2O_3 (22–641).

band at 670 cm^{-1} appeared and it was attributed to Ru(III) that strongly interacts with La.[12] LRS has been used to study the oxidation of ruthenium films at atmospheric pressure.[29] RuO_2, RuO_4 and RuO_3 have been detected on thermal oxidation of initially reduced Ru surface. However, only a few studies have reported the application of this technique to characterize Ru supported catalysts.[30]

The support and the calcined fresh catalysts exhibited a mixture of phases which were influenced by the metal type. However, the XRD and Raman data of the used catalysts supported on lanthanum oxide showed that only type **II** oxycarbonate was present. It is clear from these studies that independently of the phases initially present, the only remaining crystalline phase is the hexagonal form of the oxycarbonate.

No metallic Rh and Ru peaks were detected by XRD.[12,28] For all Ru solids, the Raman band at 670 cm^{-1} almost vanished (Fig. 1), in agreement with the reduced state of the samples. The presence of Pt^0 reflections in the corresponding XRD pattern indicated that Pt was sintered after more than 100 h on stream in theMR. This was probably the main cause of Pt/La_2O_3 deactivation.[11]

It has been shown that La_2O_3 can substantially modify the chemical behavior of M/SiO_2 systems.[31,32] The Rh supported on the combined La_2O_3–SiO_2 composite showed an XRD pattern similar to pure SiO_2 support calcined at 1173 K with a significant broadening at $2\theta = 28$ and 45° that corresponds to the appearance of the characteristic peaks of lanthanum disilicate phase.[13] Peaks indicating the presence of lanthanum carbonates, oxycarbonates or hydroxide were not observed in agreement with FTIR and Raman results.[13] The lanthanum disilicate could prevent the formation of detectable amounts of lanthanum

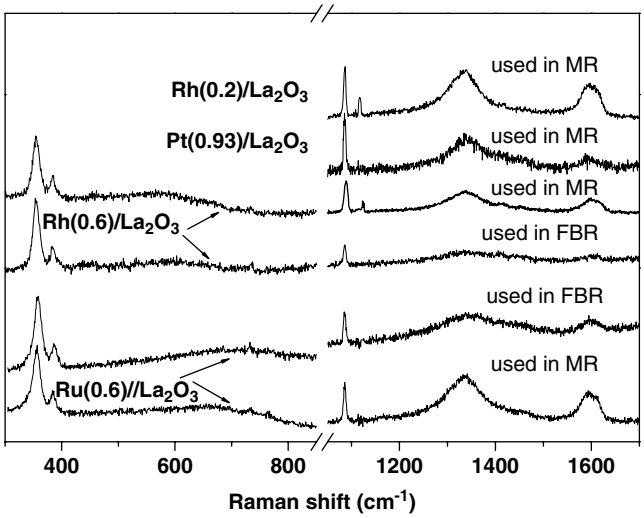

Figure 1. Laser Raman spectra for the catalysts after CO_2 reforming of methane at 823 K in a fixed-bed reactor and a membrane reactor.

oxycarbonates even after a long time on stream. However, Diffuse Reflectance Infrared Fourier Transform Spectroscopy (DRIFTS) and TPD experiments support the presence of some sort of carbonate species.[33] It has been estimated that 2% of the La_2O_3 load could be available to form carbonates in the presence of carbon dioxide.

Carbon deposits

Different types of deactivating coke deposits have been reported for methane reforming on metal catalysts such as adsorbed atomic carbon, amorphous carbon,

© 2009 Curtin University of Technology and John Wiley & Sons, Ltd.

DOI: 10.1002/apj

bulk carbide, filamentous and crystalline graphitic carbon.[8,10] For all the used La-based catalysts, no carbon deposition was observed through TGA measurements. Raman spectroscopy is a sensitive technique to study the properties of carbon nanotubes, carbonaceous particles, carbon films, synthetic diamond and catalytic carbon. The Raman spectra of the various forms of graphite have been discussed extensively in the literature.[34] The first-order transitions lie between 1200 and 1700 cm^{-1}.

The Raman spectra of hexagonal crystal graphite[34,35] consist of the main first-order band (G band at 1580 cm^{-1}) assigned to the in-plane displacement of carbon atoms in the hexagonal sheets. When disorder is introduced into the graphite structure, the existing bands broaden and additional bands are found at about 1350 cm^{-1} (D mode) and 1620 cm^{-1} (D′ mode). In the rather small or disordered crystal with very little three-dimensional order, the G and D′ bands merge into a single broader feature. The G peak indicates the presence of large graphite crystals, whereas the ratio of the D to G peaks gives the relative amount of edge to the volume of the crystals.

For the catalysts supported on La_2O_3 used in the FBR, a group of very low-intensity and broad Raman bands at 1340 and 1590 cm^{-1} was observed (Fig. 1). In the case of the catalysts used in theMR, the Raman band intensities increased, and the peaks were better defined. It was previously reported[28] that these solids evaluated at higher W/F (near the thermodynamic equilibrium) in a MR exhibited higher intensity bands due to the larger amounts of graphitic carbon being formed. This phenomenon could be due to different factors; one of them may be the increase in CO concentration that favors the CO disproportionation reaction. Note that all the catalysts were exposed to similar amounts of reactants during 180 h on stream in the MR.

The D band is more intense than the G band for all carbonaceous species formed on the different catalysts used in the MR. The spectra were fitted using Lorentzian line shapes at the frequencies of D, G and D′ transitions. The Raman band intensities were calculated. Figure 2 shows the fitted spectrum for the used $Rh(0.6)/La_2O_3$ as an example. The small signals appearing at 1400 cm^{-1} are due to the oxycarbonates.

For the Rh and Pt catalysts, the high-D/G relative intensity (D/G = 3.3–11.2) at low-W/F ratios indicates that the crystallization order is a function of the contact time (space velocity). The D/G ratios obtained for the Ru catalysts (D/G ~4) used in a MR show that these catalysts contain a similar proportion of disordered carbon.[12] No graphitic carbon bands were detected for the used Rh catalyst supported on the La_2O_3–SiO_2 support.

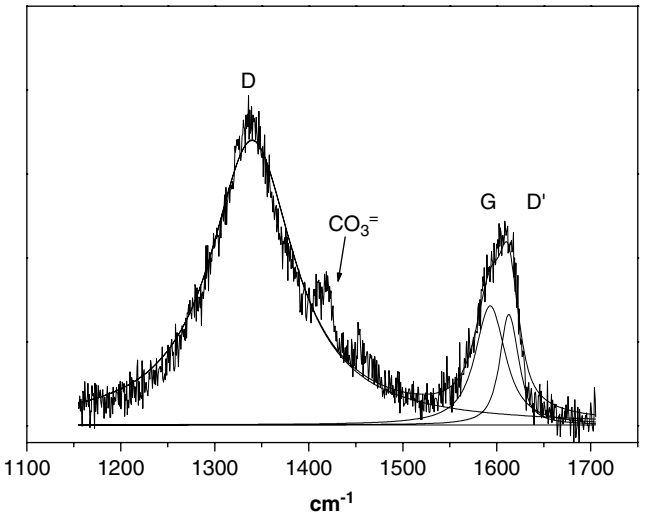

Figure 2. Laser Raman spectrum of $Rh(0.6)/La_2O_3$ solid after 180 h on stream in the membrane reactor fitted using Lorentzian curves located at the frequencies of the D,G and D′ bands.

In the M/La_2O_3 catalysts, the carbon deposits did not significantly affect the activity in the MR. This behavior could be related to the sites on which carbon is deposited and/or to the role as reaction intermediate that carbon would play. The observations derived from our characterization results lead us to propose a reaction step for our noble metal–lanthanum based system that resembles the one proposed by Verykios *et al*.[36] for Ni/La_2O_3.

The precise role to $La_2O_2CO_3$ in the reaction mechanism can be written as follows:

$$La_2O_2CO_3 + C - S \xrightarrow{k_4} La_2O_3 + 2CO + S$$

This slow reaction most likely occurs at the metal/support interface.

Reducibility of catalysts prepared on different lanthanum-containing supports

After treatment in flowing oxygen at 823 K to release the adsorbed water and CO_2, the TPR experiments were performed. The TPR profiles of Rh catalysts supported on lanthanum oxide showed two main peaks between 420 and 490 K (Table 2), independently of the Rh loading. A weak shoulder was observed at 405 K. The reduction temperature of the Rh/La_2O_3 catalysts, which was significantly higher than for the Rh/SiO_2 solid (maximum reduction temperature = 405 K), indicates that there is a strong interaction between rhodium and the La_2O_3 support.[10] An intermediate situation occurs with the Rh supported on La_2O_3–SiO_2: the TPR profiles

© 2009 Curtin University of Technology and John Wiley & Sons, Ltd.

DOI: 10.1002/apj

Table 3. Binding energies[a] and surface atomic ratios of calcined solids and after dry reforming in a fixed-bed reactor.

Samples	Treatment	M $3d_{5/2}$ (eV)	O 1s[a] (eV)	M/La+Si	O/La	$CCO_3^=$/La	$CCO_3^=$/O
$Rh(0.6)/La_2O_3$	Calcined	308.1 (3.1)[b]	530.1 (90)[c] 528.0 (10)	0.46	1.6	1.6	1.0
	Used	306.1 (2.0)	530.1 (80) 527.5 (20)	0.41	2.3	0.87	0.5
$Rh(0.6)/La_2O_3-SiO_2$	Calcined	308.8 (3.4) 306.4 (3.1)	531.6 (100)	0.0027	–	–	–
	Used	307.1 (3.8)	531.8 (100)	0.0027	–	–	–
$Ru(0.6)/La_2O_3$	Calcined	283.4 282.3	531.8 (89) 528.7 (11)	0.10	2.71	0.60	0.22
	Used	283.4[d] 282.3[d] 280.2	531.1 (78) 528.8 (22)	0.12	3.75	0.89	0.24
$Ru(1.2)/La_2O_3$	Calcined	283.4 282.3	531.0 (76) 528.7 (24)	0.18	2.91	0.55	0.19
	Used	283.4[d] 282.3[d] 280.4	531.4 (82) 528.9 (18)	0.17	3.63	0.97	0.26

[a] Contamination carbon was taken as reference at 284.6 eV.
[b] FWHM are given between parentheses.
[c] The relative intensity of oxygen species is given between parentheses.
[d] Low-intensity peaks.

show a sharp single peak at 420 K, suggesting a weaker Rh–La interaction.[13]

$Ru(0.6)/La_2O_3$ catalyst[12] exhibits a main reduction peak at 533 K, a second one at 648 K and a low-intensity shoulder at 413 K. However, for Ru(1.2), a high-intensity peak appears at 481 K with a significant shoulder at 533 K while the peak at 413 K becomes well defined.

We prepared a Ru/Al_2O_3 catalyst to help in the identification of the Ru species present on Ru/lanthanum catalysts; however, we did not evaluate its catalytic activity. The TPR profile for this solid only shows a main feature at 373 K. Taking into account that the XRD pattern exhibits the main reflections of the monoclinic RuO_2 oxide, the low temperature TPR feature could be assigned to the RuO_2 crystalline phase in the Ru/alumina catalyst. Then, the high-temperature peak at 533 K in Ru(0.2) and $Ru(0.6)/La_2O_3$ solids suggests the existence of a strong metal–support interaction. And the very low intensity of the 413 K peak is in agreement with the low dispersion of all the Ru solids.

In the case of Rh/La_2O_3 based catalysts, the strong metal–support interaction was the basis of their high stability. This strong interaction is related to the chemical affinity of Rh to form rhodates. In a similar way, Ru can form complex, mixed oxides with perovskite structure. From the hydrogen consumption results, the μmol H_2/μmol metal ratios were calculated. For all catalysts, this ratio was ~1.50, indicating a metal oxidation state of **III**. In the case of the Pt/La_2O_3 solid, the presence of several TPR peaks suggests different types of metal-surface species. The H_2/Pt molar ratio was close to 2 indicating that Pt(IV) was present.[11]

Surface characterization

The stable Rh and Ru catalysts after calcinations and after use in the CO_2 reforming of methane at 823 K were characterized by XPS. The intensity ratios and binding energies are summarized in Table 3.

Values in the 307.6–309.6 eV range for Rh^+ compounds have been compiled by Nefedov *et al*.[37] However, Gysling *et al*.[38] have reported Binding Energies (BEs) for Rh^{2+} compounds within a similar range (308.4–309.3 eV). The Rh^{3+} oxidation state presents a binding energy of 309.7 eV and for pure Rh metal foil, a Rh $3d_{5/2}$ peak appears at 307.0 eV, with 1.6 eV Full width at high maximum (FWHM).[39]

For the Rh calcined solids, the Rh 3d peaks present a FWHM between 3.1 and 4.8 eV, suggesting a mixture of Rh oxidation states. The high-binding energy values indicate the presence of Rh^{n+} species.[22,33]

The used catalysts showed a line width and a binding energy lower than those of the calcined samples, indicating reduction to Rh^0. The FWHM of the Rh $3d_{5/2}$ peak mainly reflects the particle size.[40] The increased FWHM for small particles, where the BE is also sensitively size dependent, originates from the particle size distribution. In the case of the used $Rh(0.6)/La_2O_3$ catalyst, the FWHM was 1.8 eV;

© 2009 Curtin University of Technology and John Wiley & Sons, Ltd.

DOI: 10.1002/apj

however, for the used $Rh(0.6)/La_2O_3-SiO_2$ solid, the FWHM was significantly higher (3.7 eV), suggesting a smaller Rh average particle size in this sample. The Rh/La surface atomic ratio slightly decreases for the Rh/La_2O_3 solid, and the Rh/La+Si ratio remains constant for the $Rh/La_2O_3-SiO_2$ indicating that no change in the rhodium dispersion has occurred for both types of catalysts. This is consistent with the high catalytic stability of these solids.

In the case of Ru, there is an overlap between Ru 3d and C 1s peaks at 284.8 eV. For the calcined solids, two Ru $3d_{5/2}$ peaks could be observed at 282.3 eV and 283.4 eV.[12] Elmasides *et al*. and Tsisun *et al*.[41,42] attributed a binding energy of 284.0 eV to Ru(IV) species deposited onto the alumina surface. Elmasides *et al*.[41] assigned the Ru species at 282 eV to Ru(IV)/Ru(III) oxyhydrates, Ru^{+2} on Al_2O_3 and Ru^{+} in Y zeolite. In our Ru supported on lanthanum oxide solids, the Laser Raman peak at 670 cm^{-1} suggested the presence of Ru(III) species that strongly interact with La. This result is in agreement with the appearance of the 282 eV BE peak in the XPS spectra of calcined solids that could be assigned to Ru(III).

Verykios *et al*.[41] found that on alumina, ruthenium is incompletely reduced by treatment with H_2 at 823 K while on TiO_2, Ru is more easily reduced to the metallic state. They found that the chemical behavior strongly depends on the material on which it is supported. For the mixed $LaRu_{1-x}Ni_xO_3$ perovskite-type oxides, two peaks of Ru $3d_{5/2}$, one at ≈280 eV attributed to Ru^0 and a second one at ≈282.6 eV corresponding to unreduced Ru (Ru(III)), were reported by Goldwaser *et al*.[43]

For our Ru used catalysts, a Ru^0 peak at 280.2 eV appeared together with low proportions of higher BE peaks. On the other hand, the Ru/La atomic ratio slightly changed compared with the calcined sample, indicating that the ruthenium dispersion remains constant after being used in the MR.

For all samples, dispersion values lower than 5% were obtained from CO and H_2 chemisorption results. The low chemisorption after a high-temperature reduction is probably not indicative of the real dispersion due to the occurrence of a strong interaction between the metal and the support.[40,44]

For all catalysts supported on lanthanum oxide, the C 1s spectra exhibit a well-defined peak at 289.3 eV that was attributed to carbonate carbon.[45] The $CCO_3^{=}$/La ratios were similar for the used catalysts, due to the oxycarbonate formation during reaction. However, for the $Rh(0.6)/La_2O_3-SiO_2$ solid, the C 1s spectra only show one well-defined peak at 284.4 eV and no peak at 289.1 ± 0.2 eV related to surface oxicarbonate was observed, in agreement with LRS and FTIR results.

MR data

Different approaches to describe the optimal performance of MRs have been reported in the literature.[46,47] In general, it is necessary to balance the feed, reaction and permeation rates. It has been noted that for the optimal performance of a MR, the rate ratio ($R_{CH_4}/R_{H_2\ permeation}$) should take values between 0.1 and 10.[6] This parameter accounts for the ability of the reactor to convert CH_4 and to transport H_2. The high activity of the catalyst is important to restore the reaction equilibrium; besides, the permeation rate should be high enough to eliminate the H_2 produced. If the catalyst is of low activity, equilibrium is approached too slowly, so that removal of the hydrogen produced will not affect the yield.

For the most active Rh and Pt catalysts, a significant improvement in the methane conversion was obtained using the MR (Fig. 3). In addition, the measured $R_{CH_4}/R_{H_2\ permeation}$ ratio values (between 1.8 and 5.0) were within the margins of good performance.

Regarding the approach to equilibrium of the dry reforming reaction,[13,46,47] one can define a fraction of reaction equilibration (η) using the following equation:

$$\eta = \frac{\prod p_i^{vi}}{K_{eq}}$$

where p_i is the measured partial pressure of each reactant and product in the reaction side of the MR, v_i the stoichiometric numbers for the $CO_2 + CH_4$ reaction and K_{eq} the experimental equilibrium constant (evaluated in the FBR operation mode that is close to the theoretical value). If the composition corresponds to thermodynamic equilibrium, this ratio will equal 1.

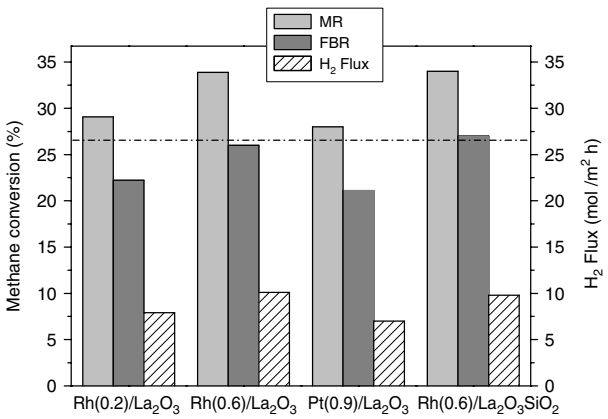

Figure 3. Comparison of the methane conversion and the hydrogen flux on the Rh and Pt catalysts at W/F = 5×10^{-4} g h ml^{-1}. T = 823 K. Sweep gas flow rate = 10 ml min^{-1}. Permeation area = 3×10^{-4} m^{-2}. The dotted line indicates the thermodynamic value considering the dry reforming and the RWGS reactions.

© 2009 Curtin University of Technology and John Wiley & Sons, Ltd.

DOI: 10.1002/apj

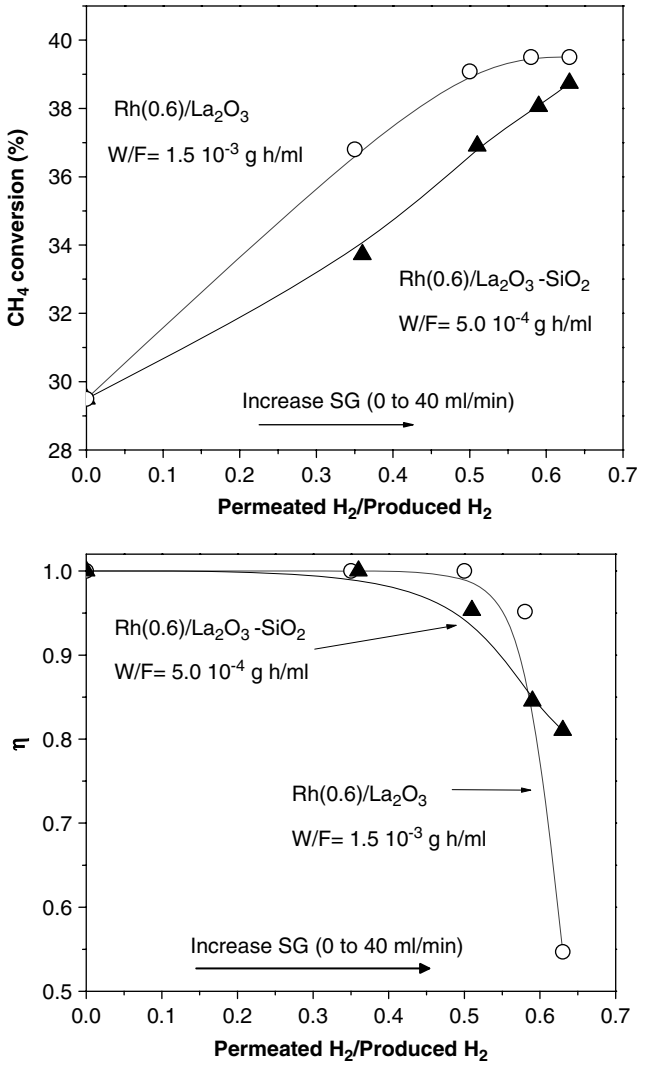

Figure 4. Variation of the methane conversion and the equilibration reaction ratio for the dry reforming reaction with the permeated H_2/produced H_2 ratio. $T = 823$ K, $\Delta P = 0$ Pa, permeation area $= 3 \times 10^{-4}$ m^{-2}. $\left(\eta = \frac{\prod_i p_i^{vi}}{K_{eq}} \right)$.

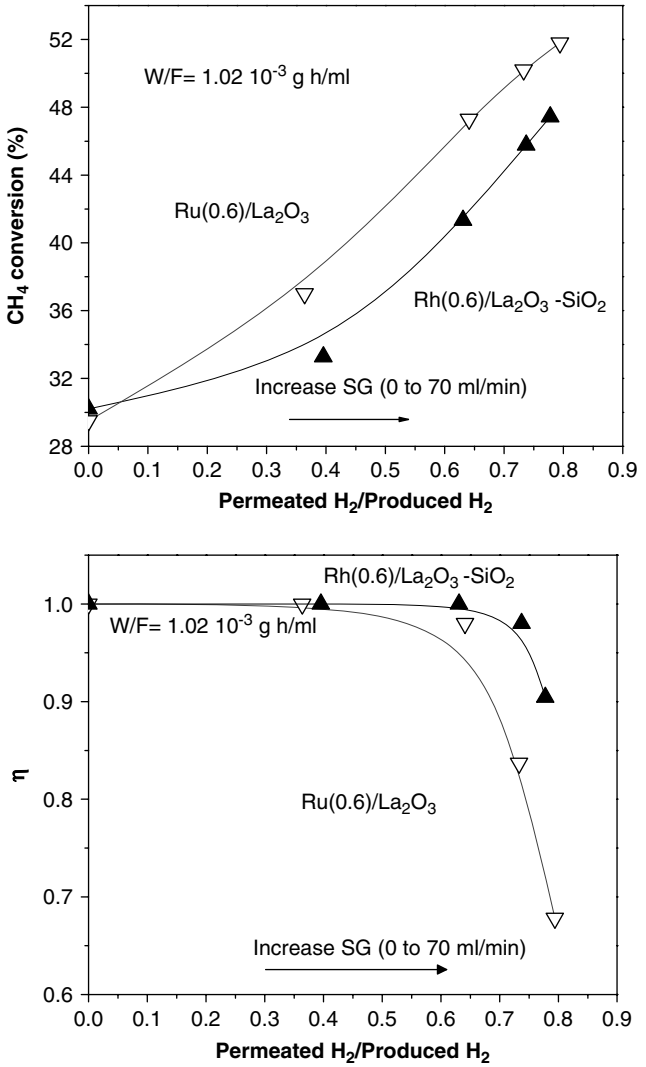

Figure 5. Variation of the methane conversion and the equilibration reaction ratio for the dry reforming reaction with the permeated H_2/produced H_2 ratio. $T = 823$ K, $\Delta P = 0$ Pa, permeation area $= 5 \times 10^{-4}$ m^{-2} $\left(\eta = \frac{\prod_i p_i^{vi}}{K_{eq}} \right)$.

The CH_4 conversion and η as a function of the ratio between the permeated H_2 and the H_2 produced (hydrogen recovery) are shown in Figs. 4 and 5. The permeated H_2 and the H_2 produced ratio increases with the SG flow rate. Two different permeation areas were employed. Figure 4 compares the behavior of the Rh catalysts when a permeation area equal to 3×10^{-4} m^2 was used in the MR. Both catalysts present a significant increase of methane conversion together with an effective transport of H_2 through the membrane. They exhibit a similar behavior in the reaction equilibration ratio; when the hydrogen recovery increases this ratio decreases. For the $Rh(0.6)/La_2O_3$, the reaction equilibration ratio begins to diminish when hydrogen recovery is higher than 60%. However, for the solid supported on the binary oxide operated at W/F $= 5 \times 10^{-4}$ g h ml^{-1}, the equilibration ratio changes very slowly. This is in agreement with the constant increase of methane conversion as a function of the SG flow rate. For the other solid, the conversion values remained practically constant.

The $Rh(0.6)/La_2O_3{-}SiO_2$ solid was compared with $Ru(0.6)/La_2O_3$ (Fig. 5), employing a higher permeation area (5×10^{-4} m^2) and increasing the SG flow rate to 70 ml min^{-1}. When a high hydrogen recovery was reached (close to 80%), the first solid could keep a η value equal to 0.9. This would indicate that for the most active catalyst, it would be possible to obtain a high hydrogen recovery maintaining the capacity to

© 2009 Curtin University of Technology and John Wiley & Sons, Ltd.

DOI: 10.1002/apj

restore the thermodynamic equilibrium. This behavior could be related to the good dispersion and high activity (Table 1) of the La_2O_3–SiO_2 solid.[13]

Recently, Ferreira Aparicio *et al*.[3] employed a highly selective Pd film (12–35 μm) supported on porous stainless steel and several Ni-based catalysts in a MR for the dry reforming reaction. They found that a certain CO_2 excess in the feed with respect to the stoichiometric ratio establishes more favorable conditions for the MR operation with lower carbon deposition. Under these conditions, their system produced a hydrogen permeation flux of 4.4×10^{-7} mol s^{-1} m^{-2} with a hydrogen recovery yield (H_2 permeate/H_2 produce = 0.93) of 93% for a CO_2/CH_4 ratio equal to 1.9 and a SG of 300 ml min^{-1}. However, we have obtained a higher H_2 permeation flux equal to 5.68×10^{-7} mol s^{-1} m^{-2} and a hydrogen recovery of 80% employing a $CO_2/CH_4 = 1$ and a SG of 70 ml min^{-1} (0.05 mmol s^{-1}). In both cases, a similar feed flow rate of methane ($\sim 3.3 \times 10^{-6}$ mol s^{-1}) was fed.

Of all the Ni catalysts tested by Menad *et al*.[3] the $Ni/Ce_{0.5}Zr_{0.5}O_2$ solid was the only one able to keep its surface free of carbon fibers. It should be noted that after each catalytic test, the membrane permeability was measured. The membrane did not show any variation on the hydrogen permeation rate and no visual damage or carbon deposition was observed.

MATHEMATICAL MODEL APPLIED TO RH(0.6)/La_2O_3

Reaction kinetics

In a previous work,[22] we proposed realistic intrinsic rate equations for the dry reforming using Rh(0.6)/La_2O_3 as catalyst. Different observations support a reaction mechanism in which the slow steps are the methane decomposition and the surface reaction of the lanthanum oxycarbonate with the carbon. The mechanistic picture is that methane reversibly adsorbs on the metallic clusters (K_1), while the cracking of the adsorbed species proceeds slowly liberating H_2 and generating carbon that remains on the metallic surface (k_2). The CO_2 rapidly reacts with La_2O_3 to generate oxycarbonate (K_3), which in turn reacts slowly with carbon to generate the other main product, CO (k_4). This slow reaction occurs most likely at the metal/support interface while the RWGS occurs simultaneously and is always equilibrated.

The rate equations for the following two reactions were obtained as follows:

$$CH_4 + CO_2 \leftrightarrow 2H_2 + 2CO \quad (1)$$

$$CO_2 + H_2 \leftrightarrow CO + H_2O \quad (2)$$

The corresponding rate equations are

$$r_1 = \left[\frac{K_1 k_2 K_3 k_4 P_{CH4} P_{CO2}}{K_1 K_3 k_4 p_{CH4} P_{CO2} + K_1 k_2 P_{CH4} + K_3 k_4 P_{CO2}}\right] \cdot \left[1 - \frac{(P_{CO} P_{H2})^2}{K_{eq1} \cdot P_{CH4} P_{CO2}}\right] \quad (3)$$

$$r_2 = k_5 \cdot P_{CO_2}^{0.55} \cdot P_{H_2}^{0.42} \cdot \left(1 - \frac{P_{CO} \cdot P_{H_2O}}{K_{eq2} \cdot P_{CO_2} \cdot P_{H_2}}\right) \quad (4)$$

where r_i is the rate equation for reaction i; P_j, the partial pressure for species j; K, the adsorption constants; k_i, kinetic constants; and K_{eqi}, equilibrium constant for reaction i. The values of the parameter needed to calculate the numerical values of all these constants at a given temperature are listed in Table 4 for the Rh(0.6)/La_2O_3 solid.

Hydrogen permeation rate

The hydrogen permeation rate through the membrane from the retentate side to the permeated side is assumed to obey the Sievert law.[48]

$$N_{H_2} = K_{H_2}((P_{H_2})^{0.5} - (P_{H_2}{}')^{0.5}) \quad (5)$$

where N_{H_2} is the permeation flux of hydrogen, P_{H_2} and $P_{H_2}{}'$ are hydrogen partial pressures in retentate side and permeated side, respectively and K_{H_2} is the permeance. When a 100% selective Pd–Ag membrane was used, Kj was equal to 0 for components other than hydrogen. A H_2 permeability study of the membrane was conducted in the empty reactor over a range of temperatures (673–823 K).[11]

Table 4. Arhenius parameters for dry reforming and water gas shift reaction measured for Rh(0.6)/La_2O_3.

Constants	A Unit	A Value	Δhr (kcal/mol)	E_A (kcal/mol)
K_1[a]	kPa^{-1}	14.0	7.8	–
k_2[b]	mol (g s)$^{-1}$	2.44	–	16.9
K_3[c]	kPa^{-1}	4.85×10^{-8}	34.8	–
k_4[d]	mol (g s)$^{-1}$	2.47×10^{5}	–	41.2
K_5[e]	mol (g s)$^{-1}$	8.2×10^{-3}	–	9.8
K_{eq1}[f]	kPa^2	4.81×10^{18}	61.8	–
K_{eq2}[g]	–	29.59	8.0	–

[a] Equilibrium constant of methane adsorption.
[b] Rate constant of the decomposition of methane.
[c] Equilibrium constant of the reaction between CO_2 and La_2O_3, from Shirsat *et al*.[49]
[d] Rate constant of the reaction between the oxycarbonate species and carbon.
[e] Rate constant of water gas shift reaction.
[f] Equilibrium constant of water gas shift reaction.
[g] Equilibrium constant of dry reforming reaction (dimensionless).

© 2009 Curtin University of Technology and John Wiley & Sons, Ltd.

DOI: 10.1002/apj

Model development

The modeling of MRs presents interesting challenges because of the coupling of selective diffusion through the permeated surface with chemical reactions and mass transfer on the reactor side. A model predicting product distribution is necessary.

In this work, a tube and shell reactor configuration was used; the packed bed was held in the shell side. The following assumptions were incorporated for the mathematical model:

1. The internal mass transfer resistance of the packed catalyst was neglected due to the small catalyst particles.
2. One-dimensional tubular reactor with no radial concentration and temperature gradient and axial dispersion on both the tube and shell sides, and no gas film resistance to heat and mass transfer at the membrane walls. These effects can be minimized by selecting the appropriate ratio of catalyst bed length to particle size. Mears[50] established the following criterion for the minimum reactor (L/d_p) necessary to avoid significant axial gradients in concentration.

$$\frac{L}{dp} \triangleright 92\mathrm{N_{Rep}}^{-0.23} n \ln \frac{1}{(1-x)}$$

The inequality for the study conducted here was $11.36 \gg 3.45 \times 10^{-3}$, this value establishing that axial gradients were insignificant and that plug – flow occurred in the bed.

Mass balance

A mass balance for a differential reactor volume along the z-axis of both the FBR and the MR (Fig. 6) has been written for the reaction zone and for the permeation zone (for the MR only).

Reaction zone (shell side)

$$\frac{dQ_\mathrm{i}}{dz} = \frac{W_C}{V_r} \sum_{\mathrm{j}=1}^{2} \upsilon_\mathrm{i} r_\mathrm{i} + 2\frac{N_\mathrm{i} R_1}{(R_3^2 - R_2^2)} \qquad (6)$$

Permeation zone (tube side)

$$\frac{dQ'_\mathrm{i}}{dz} = 2\frac{N_\mathrm{i}}{R_2 - R_1} \qquad (7)$$

where Qi and Q'_i are the axial molar flow rate of the ith species of retentate side and permetate side, respectively, W_C is catalyst weight, V_r is reactor volume, υ_i and r_i are stoichiometric coefficient and reaction rate for reactions (1) and (2), R_1 and R_2 are inner radius of the SG tube and of the permeation tube membrane, respectively and R_3 is inner radius of the shell.

The system of differential equations was solved using the Bulirsch-Stoer (Bulstoer) method available in package Mathcad Proffessional 2000. Reaction conditions and parameters are summarized in Table 5.

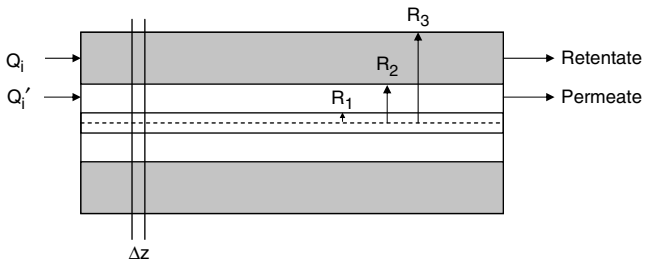

Figure 6. Schematic diagrams of the cross-section of the dense membrane reactor.

Table 5. Reaction conditions and reactor parameters used in the simulation.

Feed Composition	CH_4: CO_2: Ar = 1 : 1 : 1.1
Reactor temperature	823 K
Pressure for both tube and shell side	10 1324 Pa
Catalyst weight (W_C)	1.5 g
Outer radius of sweep gas tube (R_1)	7.93×10^{-4} m
Inner radius of tube (R_2)	1.58×10^{-3} m
Inner radius of shell (R_3)	4.76×10^{-3} m
Length of the reactor	0.03 m
Membrane area	3×10^{-4} m^2
Hydrogen Permeance	1.35×10^{-4} mol/(m^2 s Pa$^{0.5}$)

Comparison between model and experimental data

An important parameter that influences the performances of the MR is the SG flow rate. Figure 7 shows the effect of SG flow rate on both the methane and carbon dioxide conversion for the Rh(0.6)/La_2O_3 catalyst. Increasing the SG flow increases both reactant conversions; however, the CO_2 conversion increase is lower than the CH_4 conversion increase because in this type of systems, the occurrence of the RWGS reaction is not favored. This is due to the reduction of hydrogen partial pressure in the permeate side, increasing the driving force for permeation and resulting in the higher rates of hydrogen removal from the reaction zone. The increase in both conversions and permeate H_2 becomes relatively small as the SG flow increases. This could be due to

© 2009 Curtin University of Technology and John Wiley & Sons, Ltd.

DOI: 10.1002/apj

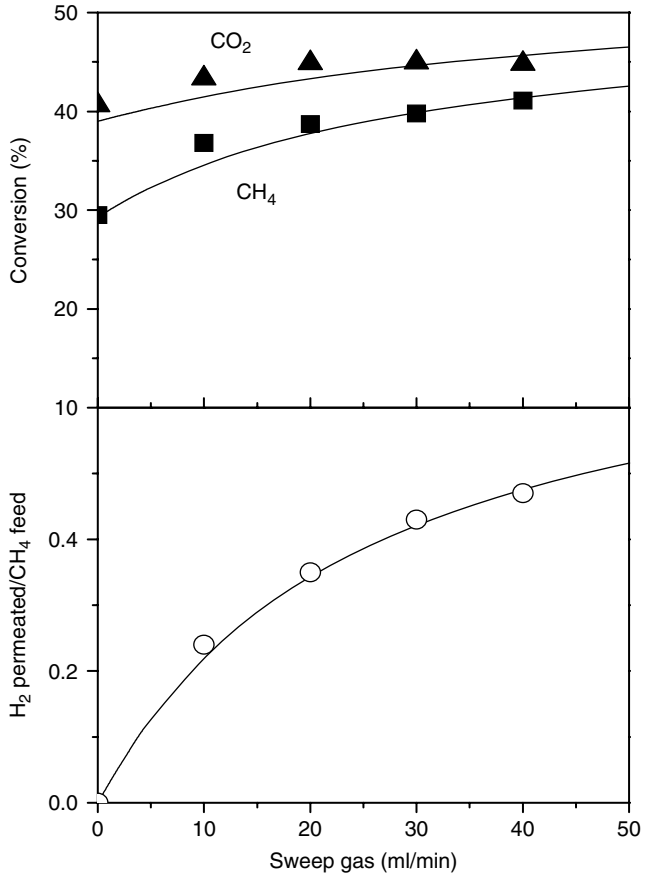

Figure 7. Effect of sweep gas flow rate on methane conversion and permeated hydrogen. Comparison of theoretical and experimental results for Rh(0.6)/La_2O_3 solid. W/F = 1.5×10^{-3} g h ml^{-1} $T = 823$ K, $P = 1$ atm.

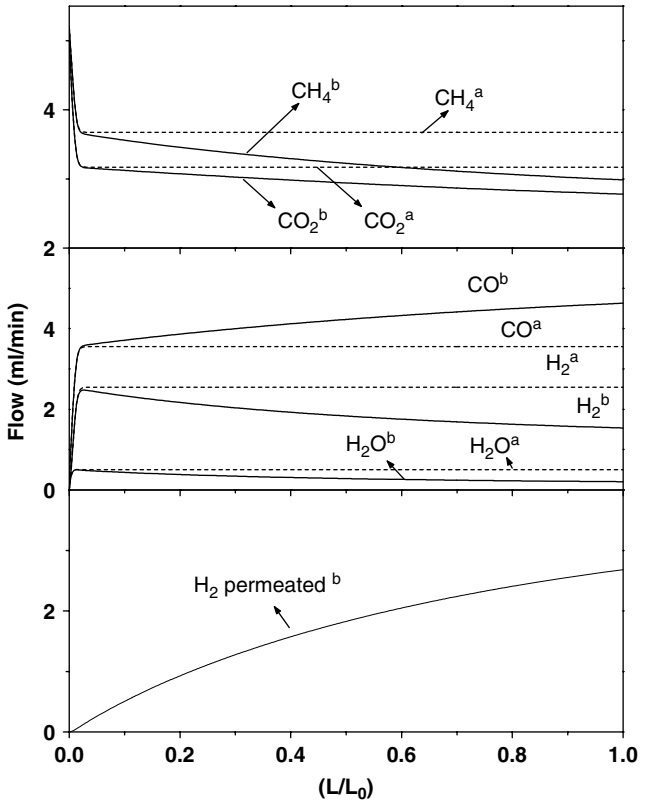

Figure 8. Shell and tube side reactant and product flow rates for fixed-bed[a] and membrane reactor[b]. W/F = 1.5×10^{-3} gh ml^{-1}, SG = 10 ml/min, T = 823 K, P = 1 atm.

the limited experimental membrane area used and the low hydrogen permeation flux.

We have compared the results from the mathematical models of dry reforming reaction in the MR with the experimental results for different SG flow rates. No similar comparison has been previously published for this reaction. The simulation results fit the experimental values fairly well under all conditions. The solid lines represent the results estimated by the model, and the data points are also shown. The good fit is an indication of the ability of the model to predict the MR behavior.

Figure 8 shows the calculated species flow rates for reactants (CH_4 + CO_2) and the product (CO, H_2 and H_2O) for the two simulated modes of reactor operation. For the FBR, the CO_2 and CH_4 flow rates decrease down the length of the reactor; in the MR, both flow rates decrease more than in the FBR. Figure 8 shows the reaction products; the CO levels are higher in the MR than in the FBR. However, the flow rates of H_2 and the hydrogen containing species (water, methane) exhibit a higher decrease in the shell side of the MR in comparison with the values obtained in the FBR. This behavior is due to the high selectivity of the Pd-Ag membrane, only H_2 passes through.

CONCLUSIONS

- A comparison of activity and stability of noble metal supported on La-based oxides in a MR was performed employing the reaction equilibration ratio. The La-containing catalysts were very stable under reaction conditions while the presence of traces of graphite only detectable through LRS does not endanger membrane stability.
- In the case of Rh and Ru La_2O_3 based catalysts, the strong metal–support interaction was the basis of their high stability. The weaker Rh–lanthana interaction for the Rh/La_2O_3–SiO_2 was strong enough to maintain the solid activity and stability.
- For our most effective catalysts, we obtained high H_2 permeation fluxes and a hydrogen recovery of 80%, employing a $CO_2/CH_4 = 1$ and high SG flow rates. Even though high hydrogen recovery was reached, the solids could keep a reaction equilibration ratio near unity, indicating that they are still able to

© 2009 Curtin University of Technology and John Wiley & Sons, Ltd.

DOI: 10.1002/apj

maintain the capacity to restore the thermodynamic equilibrium.

- A model was developed with the following assumptions: steady state operation, plug-flow behavior, isobaric conditions and negligible radial and intraparticle gradients. The results from the mathematical model of dry reforming reaction in the MR fit the $Rh(0.6)/La_2O_3$ experimental values fairly well, showing the ability of the model to predict the reactor behavior when the SG flow rate is modified.

Acknowledgements

The authors wish to acknowledge the financial support received from UNL, CONICET and ANPCyT. They are also grateful to the Japan International Cooperation Agency for the donation of the major instruments used in this study. Thanks are also given to Prof. Elsa Grimaldi for editing the language of this article.

REFERENCES

[1] E. Kikuchi, Y. Chen. *Stud. Surf. Sci. Catal.,* **1997;** *107*, 547–553.
[2] B.S. Liu, C.T. Au. *Catal. Lett.,* **2001;** *77*, 67–74.
[3] P. Ferreira-Aparicio, M. Benito, S. Menad. *J. Catal.,* **2005;** *231*, 331–343.
[4] L. Paturzo, F. Galluci, A. Basile, G. Vitulli, P. Pertici. *Catal. Today,* **2003;** *82*, 57–65.
[5] D. Lee, P. Hacarlioglu, S.T. Oyama. *Top. Catal.,* **2004;** *29*, 45–57.
[6] R. Hughes. *Membr. Technol.,* **2001;** *131*, 9–13.
[7] P. Ciavarella, D. Casanave, H. Moueddeb, S. Miachon, K. Fiaty, J.A. Dalmon. *Catal. Today,* **2001;** *67*, 177–184.
[8] M.C.J. Bradford, M.A. Vannice. *J. Catal.,* **1998;** *173*, 157–171.
[9] P.K. Cheekatamarla, C.M. Finnerty. *J. Power Sources,* **2006;** *160*, 490–499.
[10] S. Irusta, L. Cornaglia, E. Lombardo. *J. Catal.,* **2002;** *210*, 7–16.
[11] J. Múnera, S. Irusta, L. Cornaglia, E. Lombardo. *Appl. Catal. A: Gen.,* **2003;** *245*, 383–395.
[12] B. Faroldi, C. Carrara, E.A. Lombardo, L.M. Cornaglia. *Appl. Catal. A: Gen.,* **2007;** *319*, 38–46.
[13] S. Irusta, J. Múnera, C. Carrara, E.A. Lombardo, L.M. Cornaglia. *Appl. Catal. A: Gen.,* **2005;** *287*, 147–158.
[14] W.H. Casinelli, L. Feio, J.C.S. Araújo, C. Hori, F.B. Noronha, C.M. Marques, J.M.C. Bueno. *Catal. Lett.,* **2008;** *120*, 86–94.
[15] Y. Cui, H. Zhang, H. Xu, W. Li. *Appl. Catal. A: Gen.,* **2007;** *331*, 60–69.
[16] C. Batiot-Dupeyrat, G. Valderrama, A. Meneses, F. Martínez, J. Barrault, J.M. Tatibouët. *Appl. Catal. A: Gen.,* **2003;** *248*, 143–151.
[17] M.E. Rivas, J.L.G. Fierro, M.R. Goldwasser, E. Pietri, M.J. Pérez-Zurita, A. Griboval-Constant, G. Leclercq. *Appl. Catal. A: Gen.,* **2008;** *344*, 10–19.
[18] S.M. Lima, J. Assaf, M.A. Pena, J.L.G. Fierro. *Appl. Catal. A: Gen.,* **2006;** *311*, 94–104.
[19] J.S. Oklany, K. Hou, R. Hughes. *Appl. Catal. A: Gen.,* **1998;** *170*, 13–22.
[20] F. Gallucci, A. Basile. *Int. J. Hydrogen Energy,* **2008;** *33*, 1671–1687.
[21] A.K. Prabhu, A. Liu, L.G. Lovell, S.T. Oyama. *J. Membrane Sci.,* **2000;** *177*, 83–95.
[22] J.F. Múnera, S. Irusta, L.M. Cornaglia, E.A. Lombardo, C.D. Vargas, M. Schmal. *J. Catal.,* **2007;** *245*, 25–34.
[23] M. Sigl, M.C.J. Bradford, H. Knözinger, M.A. Vannice. *Topics Catal.,* **1999;** *8*, 211–222.
[24] S. Yokota, K. Okumura, M. Niwa. *Catal. Lett.,* **2002;** *84*, 131–134.
[25] R. Paul Taylor, G. Schrader. *Ind. Eng. Chem. Res.,* **1991;** *30*, 1016–1023.
[26] R.P. Turcotte, J.O. Sawyer, L. Eyring. *Inorg. Chem.,* **1969;** *8*, 238–246.
[27] S. Irusta, L.M. Cornaglia, E.A. Lombardo. *Mater. Chem. Phys.,* **2004;** *86*, 440–447.
[28] L.M. Cornaglia, J. Múnera, S. Irusta, E. Lombardo. *Appl. Catal. A: Gen.,* **2004;** *263*, 91–101.
[29] Ho Yeung H. Chan, C.G. Takoudis, M.J. Weaver. *J. Catal.,* **1997;** *172*, 336–345.
[30] Q.G. Yan, T.H. Wu, W.Z. Weng, H. Toghiani, R.K. Toghiani, H.L. Wan, C.U. Pittman Jr. *J. Catal.,* **2004;** *226*, 247–259.
[31] H. Vidal, S. Bernal, R.T. Baker, D. Finol, J.A. Pérez Omil, J.M. Pintado, J.M. Rodríguez-Izquierdo. *J. Catal.,* **1999;** *183*, 53–62.
[32] H. Vidal, S. Bernal, R.T. Baker, G.A. Cifredo, D. Finol, J.M. Rodríguez-Izquierdo. *Appl. Catal. A: Gen.,* **2001;** *208*, 111–123.
[33] J.F. Múnera, L.M. Cornaglia, D. Vargas César, M. Schmal, E.A. Lombardo. *Ind. Eng. Chem. Res.,* **2007;** *46*, 7543–7549.
[34] Y. Wang, D.C. Alsmeyer, R.L. McCreery. *Chem. Mater.,* **1990;** *2*, 557–563.
[35] T. Reshetenko, L. Avdeeva, Z. Ismagilov, Z. Pushkarev, S. Cherepanova, A. Chuvilin, V. Likholobov. *Carbon,* **2003;** *41*, 1605–1615.
[36] X.E. Verykios. *Int. J. Hydrogen Energy,* **2003;** *28*, 1045–1063.
[37] V.I. Nefedov, M.N. Firsov, I.S. Shaplygin. *J. Electron Spectrosc. Relat. Phenom.,* **1982;** *26*, 65–78.
[38] H.J. Gysling, J.R. Monnier, G. Apai. *J. Catal.,* **1987;** *103*, 407–418.
[39] K. Polychronopoulou, J.L.G. Fierro, A.M. Efstathiou. *J. Catal.,* **2004;** *228*, 417–432.
[40] G.R. Gallaher, J.G. Goodwin, C.S. Huang, M. Houalla. *J. Catal.,* **1993;** *140*, 453–463.
[41] C. Elmasides, D.I. Kondarides, W. Grünert, X.E. Verykios. *J. Phys. Chem. B,* **1999;** *103*, 5227–5239.
[42] E.L. Tsisun, B.K. Nefedov, E.S. Shpiro, G.V. Antoshin, K.h.M. Minachev. *React. Kinet. Catal. Lett.,* **1984;** *24*, 37–41.
[43] M.R. Goldwasser, M.E. Rivas, E. Pietri, M.J. Pérez-Zurita, M.L. Cubeiro, A. Grivobal-Constant, G. Leclercq. *J. Mol. Catal. A: Chem.,* **2005;** *228*, 325–331.
[44] S.S. Chan, A.T. Bell. *J. Catal.,* **1984;** *89*, 433–441.
[45] S. Lacombe, G. Geantet, C. Mirodatos. *J. Catal.,* **1994;** *151*, 439–452.
[46] L. Li, R.W. Borry, E. Iglesia. *Chem. Eng. Sci.,* **2002;** *57*, 4595–4604.
[47] D. Ma, C.R.F. Lund. *Ind. Eng. Chem. Res.,* **2003;** *42*, 711–717.
[48] A. Sieverts, W. Kumbhaar. *Ber Dtsch Chem. Eng. Des.,* **1910;** *43*, 893–900.
[49] A.N. Shirsat, M. Ali, K.N.G. Kaimal, S.R. Bharadwaj, D. Das. *Thermochim. Acta,* **2003;** *399*, 167–170.
[50] D.E. Mears. *Ind. Eng. Chem. Process Des. Dev.,* **1971;** *10*, 541–547.

© 2009 Curtin University of Technology and John Wiley & Sons, Ltd.